

Effect of Zirconia Morphology on Hydrodeoxygenation of Phenol over Pd/ZrO₂

Priscilla M. de Souza,^{†,‡} Raimundo C. Rabelo-Neto,[†] Luiz E. P. Borges,[‡] Gary Jacobs,[⊥] Burtron H. Davis,[⊥] Uschi M. Graham,[⊥] Daniel E. Resasco,[§] and Fabio B. Noronha^{*,†,‡}

[†]Catalysis Division, National Institute of Technology, Av. Venezuela 82, Rio de Janeiro, RJ 20081-312, Brazil

[‡]Chemical Engineering Department, Military Institute of Engineering, Praça Gal. Tiburcio 80, Rio de Janeiro, RJ 22290-270, Brazil

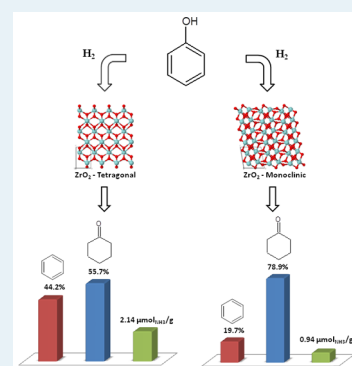
[⊥]Center for Applied Energy Research, The University of Kentucky, 2540 Research Park Drive, Lexington, Kentucky 40511, United States

[§]Center for Biomass Refining, School of Chemical, Biological, and Materials Engineering, The University of Oklahoma, 100 East Boyd Street, Norman, Oklahoma 73019, United States

Supporting Information

ABSTRACT: This work studies the effect of zirconia structure on the performance of Pd/ZrO₂ catalysts for hydrodeoxygenation of phenol at 300 °C and 1 atm using a fixed bed reactor. Benzene was the major product over Pd/t-ZrO₂, while significant formation of cyclohexanone was observed over Pd/m-ZrO₂. On the other hand, Pd/m,t-ZrO₂ exhibited intermediary behavior. DRIFTS of adsorbed pyridine, NH₃-TPD, and the dehydration of the cyclohexanol reaction revealed that the Pd/t-ZrO₂ catalyst exhibits a higher density of oxophilic sites than Pd/m-ZrO₂ and Pd/m,t-ZrO₂. This promoted the formation of deoxygenated products. However, a mechanism involving dehydration of cyclohexanol to cyclohexene, followed by dehydrogenation to benzene, may not be ruled out. Pd/ZrO₂ catalysts significantly deactivated as a function of time on stream. Results of dehydrogenation of cyclohexane and dehydration of cyclohexanol indicate that the Pd particle size increased and the density of oxophilic sites decreased during the hydrodeoxygenation of the phenol reaction. In addition, the DRIFTS spectra under reaction conditions demonstrated that the coverage of oxophilic sites by phenoxy and intermediate species increased during the reaction. The growth of Pd particles is likely responsible for the losses in the metal–support interface that gradually inhibits the ability of the adsorbed species to turnover at the metal–support boundary.

KEYWORDS: phenol, monoclinic ZrO₂, tetragonal ZrO₂, hydrodeoxygenation, biomass, bio-oil



1. INTRODUCTION

Zirconia has been reported to be a good catalyst support for various reactions due to its high thermal stability, acid–base properties, and redox surface properties.^{1,2} Generally, the catalytic performance of zirconia-based catalysts has been evaluated over reactions like alcohol dehydration,^{3,4} ketonization of carboxylic acids,^{5,6} low-temperature water–gas-shift (WGS),^{7,8} hydrosulfurization (HDS),⁹ and hydrodeoxygenation (HDO).^{10,11}

Concerning the HDO reaction, ZrO₂ support appears to favor activation of oxy-compounds on its surface, yielding mainly deoxygenation products.^{12,13} CoMoS/ZrO₂ exhibited high conversion of guaiacol to benzene, whereas ring hydrogenation products were mainly observed for CoMoS/TiO₂ or CoMoS/Al₂O₃.¹³ Mortensen et al. studied the effect of the type of support on the performance of Ni-based catalysts (Ni/ZrO₂; Ni–V₂O₅/ZrO₂; Ni–V₂O₅/SiO₂; Ni/Al₂O₃; Ni/SiO₂; Ni/MgAl₂O₄; Ni/CeO₂–ZrO₂; Ni/CeO₂; Ni/C) for the HDO of phenol in the liquid phase.¹⁴ They found that Ni/ZrO₂ was the most selective catalyst for deoxygenation products. They proposed that phenol adsorbs on coordinatively

unsaturated metal sites in the oxide surface (Zr cations) with the formation of phenoxide ion that interacts with Ni. This facilitates the hydrogenation of the aromatic ring, producing cyclohexanone, which rapidly produces cyclohexanol. This alcohol would be further dehydrated to cyclohexene, followed by hydrogenation to cyclohexane over the surface of metallic particle. Recently, our group studied the mechanism of hydrodeoxygenation of different model molecules (phenol, m-cresol) over supported Pd catalysts (Pd/SiO₂, Pd/Al₂O₃, Pd/ZrO₂).^{15,16} The Pd/ZrO₂ catalyst exhibited the highest activity and selectivity to deoxygenated products (benzene or toluene). It was proposed that the conversion of phenol (m-cresol) should involve a tautomerization step with the formation of a keto-tautomer intermediate. This highly unstable intermediate may be hydrogenated, producing cyclohexanone (3-methylcyclohexanone) and then cyclohexanol (3-methylcyclohexanol). This is the typical reaction pathway for the HDO of

Received: July 16, 2015

Revised: November 5, 2015

phenol proposed in the literature. The hydrogenation of the carbonyl group of cyclohexadienone (3-methyl-3,5-cyclohexadienone) intermediate leads to the formation of 2,4-cyclohexadienol (3-methyl-3,5-cyclohexadienol), which is in turn dehydrated to benzene (or toluene). In this case, the reaction pathway will depend on the support. For supports containing oxophilic sites such as zirconia (incompletely coordinated Zr^{4+} cations – Lewis acid sites), the carbonyl group is preferentially hydrogenated on the metal particles at the metal–support interface, leading to the formation of benzene (or toluene). Therefore, the support plays a key role in the reaction pathway.

Zirconia exhibits different crystalline structures depending on the preparation method: cubic, monoclinic, and tetragonal.^{17,18} Among the three polymorphs, cubic zirconia possesses poor stability at room temperature and thus has been less studied as a catalytic material. The tetragonal (t- ZrO_2) and monoclinic (m- ZrO_2) phases of ZrO_2 exhibit different acid/base properties^{19–21} and surface hydroxyl group concentrations.^{21,22} Therefore, the catalytic performance may be different depending on the reaction. The effects of the ZrO_2 phase on the activity and selectivity of ZrO_2 -supported Cu for methanol synthesis from CO and H_2 was studied.²³ The Cu/m- ZrO_2 catalyst exhibited a 7.5-fold higher activity for CO hydrogenation than the Cu/t- ZrO_2 catalyst. The higher activity of the Cu/m- ZrO_2 catalyst was attributed to a higher concentration of surface O atom vacancies. Such vacancies expose coordinatively unsaturated Zr cations and enhance the Brønsted acidity of adjacent Zr–OH groups, promoting the reaction of CO with OH groups that leads to formate species. Benito et al.²⁴ investigated the steam reforming of ethanol over Ni, Co, and Cu supported on zirconia with monoclinic and tetragonal phases. Nickel supported on tetragonal zirconia exhibited the best stability and selectivity for hydrogen production. The different behavior shown by m- ZrO_2 and t- ZrO_2 phases was attributed to the higher concentration of anionic defects on m- ZrO_2 than t- ZrO_2 . Rh supported on t- ZrO_2 was much more active and selective for partial oxidation of methane than Rh/m- ZrO_2 .²⁵ The authors suggested that the different strengths of interaction between metal particles and the support and different distributions of species in the metallic state on monoclinic and tetragonal zirconia may explain the better performance of tetragonal zirconia. Concerning the HDO reaction, there are only a few works that used zirconia with different structures. Hellinger et al.²⁶ studied the HDO of guaiacol over Pt supported on different metal oxides and zeolites. The following order of reactivity was found: $SiO_2 > Al_2O_3 \approx t-ZrO_2 > TiO_2$ (P25) $> TiO_2 \approx m-ZrO_2 \approx CeO_2$. Pt/t- ZrO_2 exhibited higher conversion of guaiacol and yield to cyclohexanol and methoxycyclohexanol than Pt/m- ZrO_2 . However, the authors did not explain this result. The zirconia morphology significantly affected the HDO of stearic acid over zirconia supported Ni catalysts.²⁷ Ni/m- ZrO_2 has a 3-fold times higher activity toward stearic acid hydrogenation than Ni/t- ZrO_2 . According to the proposed elementary steps, HDO of stearic acid involves the hydrogenation of stearic acid to 1-octadecanol, which is decarbonylated to C_{17} heptadecane. The higher deoxygenation activity of the Ni/m- ZrO_2 catalyst was due to the higher adsorbed concentration of the acid on m- ZrO_2 compared to t- ZrO_2 , which is related to the higher concentration of defect sites on the m- ZrO_2 surface. However, the decarbonylation rate of the alcohol to C_{17} heptadecane was the same regardless of the morphology of zirconia. Thus, the

dependency of the effect of the zirconia morphology on the reaction remains controversial.

Therefore, in the present contribution, the influence of zirconia polymorphism on HDO of the phenol reaction over Pd/ ZrO_2 catalysts is studied. Three different zirconia supports were used: monoclinic, tetragonal, and a mixture of both structures. The effect of zirconia polymorphism on the reaction pathway of HDO of phenol was investigated with diffuse reflectance infrared Fourier transform spectroscopy (DRIFTS) and catalytic tests with reactants and intermediates. Raman spectroscopy, the cyclohexane dehydrogenation and the cyclohexanol probe reactions, temperature desorption of ammonia (NH_3 -TPD), and DRIFTS of adsorbed pyridine were used to shed some light on the deactivation mechanism.

2. EXPERIMENTAL SECTION

2.1. Catalyst Synthesis. Monoclinic zirconia and tetragonal zirconia were supplied by Saint-Gobain NorPro. A ZrO_2 with a mixture of monoclinic and tetragonal phases was synthesized by a precipitation method. A solution of 2.0 mol/L of zirconyl nitrate (35 wt % $ZrO(NO_3)_2$ in dilute nitric acid, >99%, Sigma-Aldrich) was added slowly to a solution of 4.0 M ammonium hydroxide (NH_4OH , Vetec) at room temperature and kept under vigorous stirring for 30 min. The resulting precipitate was filtered and washed with distilled water until pH = 7. Then, the solid was dried at 110 °C for 12 h and calcined under dry air flow at 500 °C (heating ramp 5 °C/min) for 6 h.

The Pd-based catalysts were prepared by incipient wetness impregnation of the supports with an aqueous solution of $Pd(NO_3)_2$ (Merck) to obtain 2.0% wt of Pd. After impregnation, the sample was dried in air at 120 °C for 12 h and then calcined in air at 400 °C for 3 h (2 °C/min). The Pd/ ZrO_2 catalysts are referred to in the text as Pd/m- ZrO_2 (monoclinic zirconia), Pd/t- ZrO_2 (tetragonal zirconia), and Pd/m,t- ZrO_2 (mixture of monoclinic and tetragonal phases).

2.2. Catalyst Characterization. The chemical composition of each sample was determined using a Wavelength Dispersive X-ray Fluorescence Spectrometer (WD-XRF) S8 Tiger, Bruker with a rhodium tube operated at 4 kW. The analyses were performed with the samples (300 mg) in powder form using a semiquantitative method (QUANT-EXPRES/Bruker). Specific surface areas of the samples were measured on a Micromeritics ASAP 2000 analyzer by N_2 adsorption at the boiling temperature of liquid nitrogen. The X-ray powder diffraction (XRD) patterns were obtained on a Rigaku Miniflex diffractometer using Cu $K(\alpha)$ radiation over a 2θ range of 10–80° at a scan rate of 0.04 °/step and a scan time of 1 s/step. The Raman spectra were recorded using a Horiba LabRam HR-UV800/Jobin-Yvon Spectrometer, equipped with He–Ne laser ($\lambda = 632$ nm) with 10 mW of intensity, a CCD detector, and an Olympus BX41 microscope with objective lens of 100×. Thermogravimetric analysis of the used catalysts was carried out in a TA Instruments equipment (SDT Q600) in order to determine the amount of carbon formed over the catalyst. Approximately 10 mg of the spent catalyst was heated under air flow from room temperature to 1273 K at a heating rate of 20 K/min, and the weight change was measured.

In situ XANES experiments were performed at the D04B-XAFS – 1 beamline of the Brazilian Synchrotron Light Source (LNLS, Campinas). Typically, wafers containing pressed mixtures of the sample with BN as a binder were then placed into a sample holder located inside a quartz tubular reactor. XANES spectra at the Zr K edge (17998 eV) were successively

recorded, while the sample was heated under a 5% H₂/He mixture at 10 K·min⁻¹ up to 573 or 773 K.

The surface properties of the catalysts were investigated by temperature-programmed desorption of ammonia (NH₃-TPD). The samples (150 mg) were reduced at 573 K for 1 h under a flow of H₂ of 60 mL/min and then purged in He flow for 30 min. After reduction, the sample was cooled to 373 K, and the feed composition was switched to a mixture containing 20% NH₃ in He (30 cm³ min⁻¹) for 30 min. The physisorbed ammonia was flushed out with He flow for 1 h. Then, the catalyst was heated at 10 K/min under He to 873 K. The reactor effluent was continuously monitored by mass spectrometry.

The titration of oxophilic sites of the catalysts before and after HDO of phenol was measured by conducting the cyclohexanol dehydration reaction.²⁸ The reaction was performed in a fixed-bed quartz reactor at atmospheric pressure and 543 K. Prior to the reaction, the fresh catalyst was reduced in situ under pure hydrogen (60 mL/min) at 573 K for 1 h. The used catalysts were not exposed to air before starting the cyclohexanol reaction. The reactant mixture was obtained by flowing He (30 mL/min) through a saturator containing cyclohexanol, which was maintained at 336 K. The reaction products were analyzed by GCMS (Agilent Technologies 7890A/5975C) using an HP-Innowax capillary column and a flame-ionization detector (FID). The dehydration rate was calculated by the sum of cyclohexene, cyclohexane, and benzene yields. The nature of the acid sites was determined by DRIFTS of adsorbed pyridine. DRIFTS spectra were recorded using a Nicolet Nexus 870 spectrometer equipped with a DTGS-TEC detector. A Thermo Spectra-Tech cell capable of high pressure/high temperature operation and fitted with ZnSe windows served as the reaction chamber for in situ adsorption and reaction measurements. Scans were taken at a resolution of 4 cm⁻¹ to give a data spacing of 1.928 cm⁻¹. The number of scans taken was 512. The sample was reduced in H₂ at 573 K for 1 h and cooled to 373 K in He, and a background spectrum was recorded. Pyridine was adsorbed by bubbling He (30 mL/min) through a saturator for 30 min, followed by a He purge.

For DRIFTS of methanol adsorption, each catalyst was reduced in a 60% H₂/40% He mixture at 573 K for 1 h. The catalyst was cooled in He to 313 K, where 40 mL/min of He was flowed through a bubbler containing methanol at 300.5 K for 25 min. The catalyst was then purged in He for 25 min, during which time DRIFTS spectra (512 scans) were recorded. For DRIFTS of adsorbed CO, each catalyst was subjected to the same H₂ reduction treatment. The catalyst was cooled to 473 K. 1.3%CO in He mixture was flowed for 25 min. Spectra were recorded in flowing CO/He to measure formate band intensities by the reaction with defect-associated OH groups with CO.

The crystal size and morphology of the different ZrO₂-support and the location and size range of the Pd particles were investigated using high resolution transmission electron microscopy (HR-TEM) and scanning transmission electron microscopy (STEM) analyses. The imaging was performed using a FEI Tecnai F20 field-emission gun with an accelerating voltage of 200 kV. A symmetrical multibeam illumination was used with a Gatan Ultrascan CCD camera, a 30 mrd camera length, and a 1 nm probe size. Data processing and analysis were carried out using the Gatan Digital Micrograph software.

Catalyst powder samples were dispersed on lacy carbon copper grids.

The Pd dispersion was estimated through the dehydrogenation of cyclohexane, a structure insensitive reaction.²⁹ The dispersion of supported Pd catalysts was measured by CO chemisorption, and a correlation between the rate of cyclohexane dehydrogenation and Pd dispersion was established. This methodology was successfully used before.³⁰ This procedure enables the measurement of the Pd dispersion of fresh and used catalysts (after HDO of phenol for 20 h). Cyclohexane dehydrogenation was performed in a fixed bed reactor at atmospheric pressure over fresh and used catalysts. The fresh samples (10 mg) were first reduced at 573 K for 1 h and then cooled to the cyclohexane dehydrogenation reaction temperature (543 K). The reaction mixture (WHSV = 170 h⁻¹) was fed to the reactor after bubbling H₂ through a saturator containing cyclohexane kept at 285 K (H₂/C₆H₁₂ = 13.2). For the used catalysts, after HDO of phenol for 20 h, the saturator containing phenol was bypassed, and the reactor cooled to 543 K. Then, the cyclohexane/H₂ mixture was passed through the reactor. The exit gases were analyzed by an Agilent Technologies 7890A/5975C GCMS, using an HP-Innowax capillary column and a flame-ionization detector (FID).

In order to investigate the reaction mechanism, experiments were performed in the DRIFTS in situ cell previously described for acidity measurements under similar conditions to those employed in the HDO reaction. DRIFTS spectra were recorded using the same apparatus previously described for acidity measurements. Scans were taken at a resolution of 4 cm⁻¹ to give a data spacing of 1.928 cm⁻¹. The number of scans taken was 1024. The amount of catalyst was ~40 mg. The sample was reduced in H₂ at 573 K for 1 h and cooled to 323 K in He, and a background spectrum was recorded. Pure H₂ was then flowed through a bubbler containing phenol at 351 K, and the temperature was raised to 373, 473, 573, 673, and 773 K. To study the deactivation of the catalysts, several spectra were recorded during the steady-state HDO reaction at 573 K for 6 h.

2.3. Catalytic Activity. The vapor-phase conversion of the oxygenate compound of interest (phenol, cyclohexanol, or cyclohexanone) was carried out using a fixed-bed quartz reactor, operating at atmospheric pressure and 573 K. Prior to the reaction, the catalyst was reduced in situ under pure hydrogen (60 mL/min) at 573 K for 1 h. The catalysts were diluted with inert material (SiC mass/catalyst mass = 3.0) to avoid hot-spot formation. The reactant mixture was obtained by flowing H₂ through the saturator containing organic compound, which was kept at the specific temperature required to obtain the desired H₂/organic compound molar ratio (about 60). To avoid condensation, all lines were heated to 523 K. The reaction products were analyzed by GCMS Agilent Technologies 7890A, using an HP-Innowax capillary column and a flame-ionization detector (FID). Each of the catalysts investigated was evaluated at different W/F by varying the catalyst amount in the range of 2.5–120 mg. The W/F is defined as the ratio of catalyst mass (g) to organic feed mass flow rate (g/h). The product yield and selectivity for each product were calculated as follows:

$$\text{yield (\%)} = \frac{\text{mol of product produced}}{\text{mol of phenol fed}} \times 100 \quad (1)$$

Table 1. Pd Loading, Surface Area of the Samples, Rate of the Cyclohexane Dehydrogenation Reaction at 543 K, and Calculated Pd Dispersion of the Fresh and Used Catalysts^c

catalyst	wt % Pd	BET (m ² ·g ⁻¹)	fresh catalyst ^a		used catalyst ^b	
			reaction rate (mmol g ⁻¹ _{Pd} min ⁻¹)	D (%)	reaction rate (mmol g ⁻¹ _{Pd} min ⁻¹)	D (%)
Pd/m-ZrO ₂	2.25	103	1.01	70.0	0.40	28.2
Pd/m,t-ZrO ₂	2.24	84	0.57	40.4	0.30	21.8
Pd/t-ZrO ₂	2.13	102	0.97	67.6	0.41	28.9

^aReaction rate of dehydrogenation of cyclohexane at 543 K and calculated Pd dispersion for the fresh catalyst. ^bReaction rate of dehydrogenation of cyclohexane at 543 K and calculated Pd dispersion after HDO of the phenol reaction for 20 h. ^cAfter HDO of the phenol reaction during 20 h TOS.

$$\text{selectivity (\%)} = \frac{\text{mol of product produced}}{\text{mol of phenol consumed}} \times 100 \quad (2)$$

3. RESULTS AND DISCUSSION

3.1. Catalyst Characterization. Table 1 shows the Pd loading and the surface area of the samples and the rate of the cyclohexane dehydrogenation reaction of the fresh and used catalysts (after HDO of phenol reaction during 20 h TOS). The metal loading of the catalysts was close to the nominal values (2.0 wt %). The surface areas of Pd/m-ZrO₂, Pd/m,t-ZrO₂, and Pd/t-ZrO₂ samples were 103, 84, and 102 m²/g, respectively. The Pd dispersion of fresh Pd/m-ZrO₂ and Pd/t-ZrO₂ catalysts was quite similar (70 and 67.6%, respectively) and was 1.75 times larger than that of the Pd/m,t-ZrO₂ catalyst (40.4%). This agrees very well with the lower surface area of m,t-ZrO₂. The Pd particle size (*d*) was calculated from the dispersion data through eq 3:

$$d \text{ (nm)} = 1.12/D \quad (3)$$

The Pd particle size of Pd/m-ZrO₂ and Pd/t-ZrO₂ catalysts was 1.6 and 1.7 nm, respectively. The Pd/m,t-ZrO₂ catalyst exhibited a larger Pd particle size (2.8 nm).

The results of the HR-TEM/STEM analyses are shown in Figures 1 and 2 and indicate that the individual particle size for the t-ZrO₂ crystallites is significantly smaller compared with the m-ZrO₂ and m,t-ZrO₂ samples. This is not reflected by the BET results (Table 1), which show similar surface areas for the monoclinic and tetragonal samples and lesser surface area for the mixed (m,t) sample. Although the t-ZrO₂ crystallites are typically as small as 2–5 nm as shown in the STEM (Figure 1b), they align to form agglomerates that are very similar in size compared with the m-ZrO₂ crystals shown in Figure 1a, ranging from 5 to 20 nm, and this can certainly account for the similar BET data for the Pd/m-ZrO₂ and Pd/t-ZrO₂ support. The STEM images in Figure 1b also show that t-ZrO₂ has a more accessible surface for Pd compared with m-ZrO₂ (Figure 1a). The Pd catalyst particles hosted on the m-ZrO₂ surface were found to range from ~1.5 nm to 3.5 nm and, hence, are considerably smaller compared with the m-ZrO₂ host crystallites (Figure 1a). In contrast, the Pd particles are similar in size and difficult to distinguish from the individual t-ZrO₂ crystallites in the STEM image shown in Figure 1b. However, the Pd catalyst particles that are hosted on the larger m,t-ZrO₂ grains were found to be as large as 5 nm in size and are much less dispersed (Figure 1c). This agrees very well with the lower BET surface area that is observed for the m,t-ZrO₂ (Table 1). Furthermore, the HR-TEM imaging of the Pd/m,t-ZrO₂ catalyst provided the *d*-spacings shown in Figure 2 and illustrates that monoclinic and tetragonal domains occur side-by-side. The m-ZrO₂ form homogeneous crystals, while the t-ZrO₂ grains represent a composite of copious individual smaller crystallites

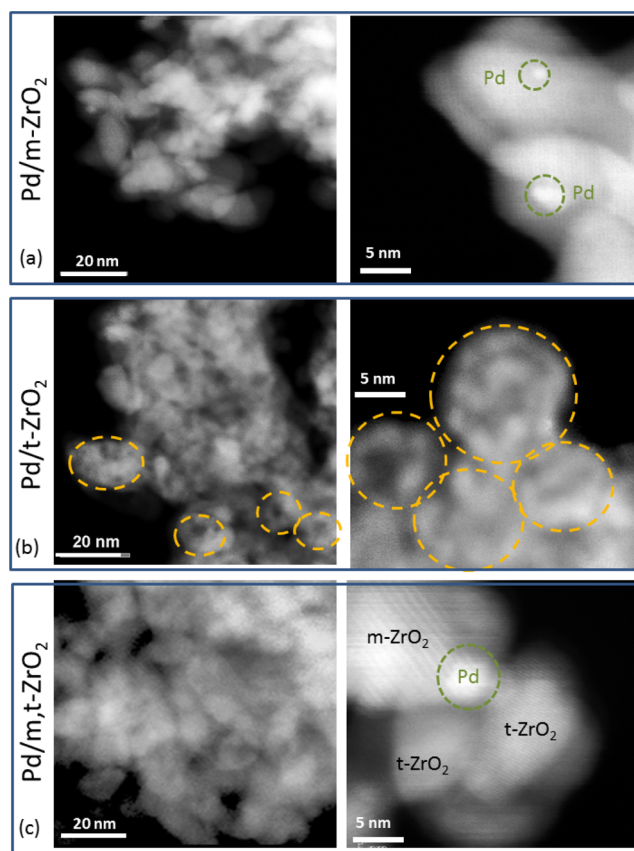


Figure 1. STEM imaging for (a) Pd/m-ZrO₂ shows particle size for ZrO₂-support grains and Pd crystallites; (b) Pd/t-ZrO₂ with small individual aligned crystallites forming a larger agglomerate support structure indicated by yellow circles; (c) Pd/m,t-ZrO₂ with juxtaposed monoclinic and tetragonal domains and large Pd crystallite.

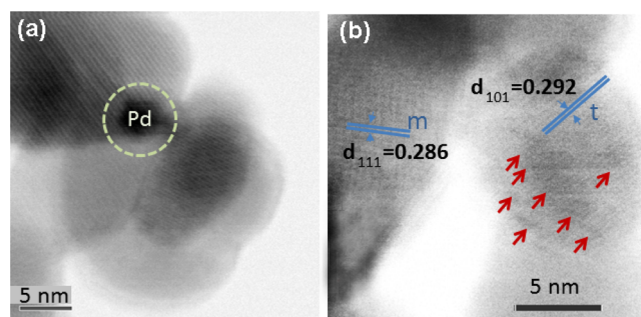


Figure 2. HR-TEM of Pd/m,t-ZrO₂: (a) shows large well crystallized m-ZrO₂ grains with ~5 nm Pd at the surface and juxtaposed to a composite grain of t-ZrO₂ crystals; (b) shows the *d*-spacings for the monoclinic and tetragonal catalyst particles. The t-ZrO₂ is a composite and includes internalized crystallites indicated with the red arrows.

(Figure 2b). The Pd particle size of the fresh catalysts measured by STEM analyses was quite similar to the ones obtained by the cyclohexane dehydrogenation reaction.

X-ray diffraction patterns for Pd/m-ZrO₂, Pd/m,t-ZrO₂, and Pd/t-ZrO₂ catalysts are shown in Figure 3. The diffractograms

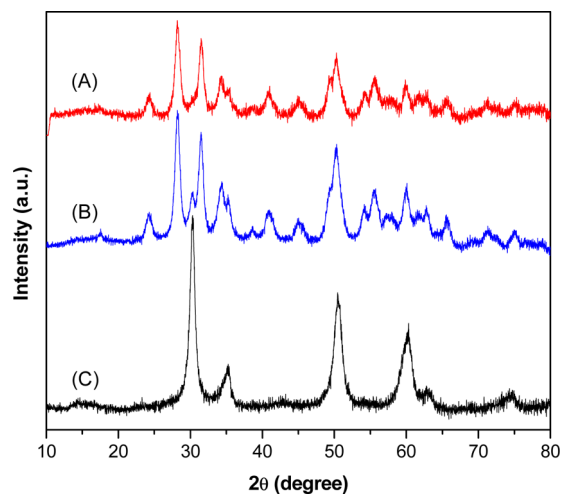


Figure 3. X-ray diffraction patterns of (A) Pd/m-ZrO₂; (B) Pd/m,t-ZrO₂; (C) Pd/t-ZrO₂.

of Pd/m-ZrO₂ and Pd/t-ZrO₂ samples display lines characteristic of monoclinic (JCPD 37-1484) and tetragonal (JCPD 17-0923) zirconia phases, respectively. The lattice parameters calculated from the diffractograms of each phase were as follows: Monoclinic: $a = 0.5297$ nm, $b = 0.5191$ nm, $c = 0.5157$ nm; Tetragonal: $a = 0.5097$ nm; $c = 0.5136$ nm. The ZrO₂ crystallite size was also calculated using the Scherrer equation, and the results obtained were 10.7 nm (monoclinic) and 9.5

nm (tetragonal). For Pd/m,t-ZrO₂, the lines typical of both phases are observed. The proportion of each phase was calculated taking into account the procedure proposed by Khaoee et al.³¹ The dominant phase is monoclinic, corresponding to 67%. The lines characteristic of PdO were not detected due to superposition with the diffraction lines of zirconia phases or to the high dispersion of PdO.

The XANES spectra at the Zr K-edge of Pd/m-ZrO₂ and Pd/t-ZrO₂ catalysts under different treatments are shown in Figure 4. The XANES spectra of calcined samples correspond to the ones typical of monoclinic and tetragonal zirconia.^{32,33} The XANES spectrum of the calcined Pd/t-ZrO₂ catalyst exhibits a white line with a double peak, which is characteristic of octahedrally coordinated zirconium.³³ In addition, it is noticed the presence of a pre-edge feature at around 18006 eV that corresponds to a $1s \rightarrow 4d$ transition, which is characteristic of compounds with distorted symmetry like tetragonal zirconia. For the Pd/m-ZrO₂ catalyst, the white line decreases immediately after the maximum absorption, and the pre-edge is not observed. The intensity of the white line decreased during reduction at 573 and 773 K, indicating that Zr⁴⁺ was partially reduced to a Zr³⁺. However, the decrease of intensity was approximately the same for both catalysts, regardless of reduction temperature. This result suggests that degree of reduction of the two polymorph catalysts was similar and, thus, the amount of Zr³⁺ cations.

The nature of acid sites was investigated by DRIFTS of adsorbed pyridine (Figure 5). The DRIFTS spectrum of adsorbed pyridine on the Pd/t-ZrO₂ catalyst showed bands at 1442, 1456, 1482, 1573, 1592, and 1602 cm⁻¹. These bands can be attributed to physically adsorbed pyridine (1442, 1456, 1482, 1573 cm⁻¹), pyridine bonded to hydrogen of the weakly acidic hydroxyl group (1592 cm⁻¹), and pyridine adsorbed on unsaturated Zr⁴⁺ cations (1602 cm⁻¹).^{34,35} The DRIFTS spectra of Pd/m-ZrO₂ and Pd/m,t-ZrO₂ catalysts were quite

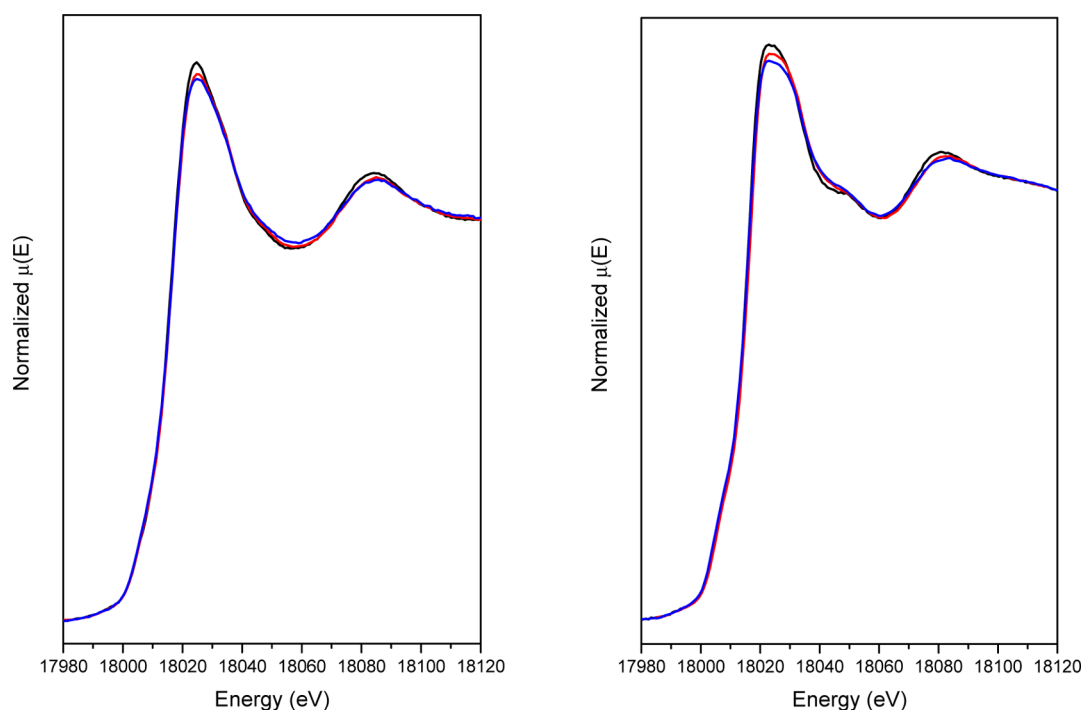


Figure 4. Normalized Zr K-edge spectra of (A) Pd/m-ZrO₂ and (B) Pd/t-ZrO₂ catalysts under different treatment. Black line: calcined sample; Red line: sample reduced at 573 K; Blue line: sample reduced at 773 K.

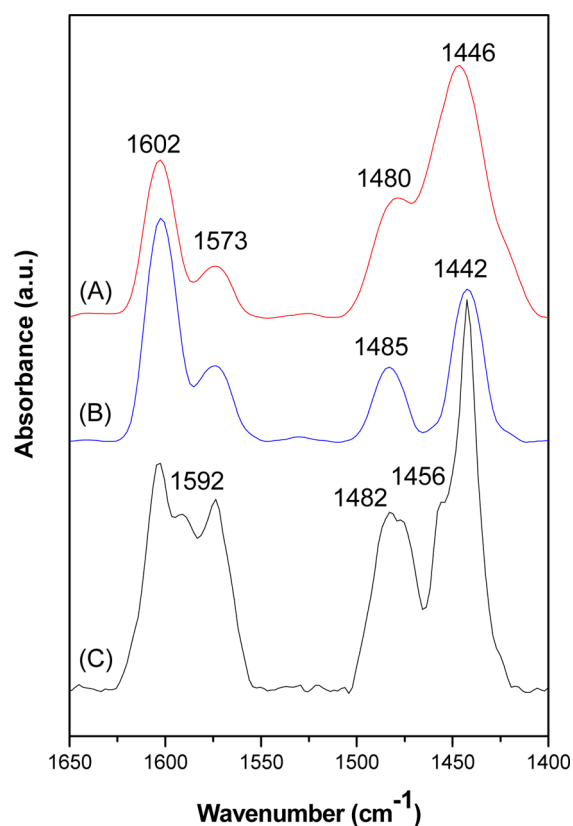


Figure 5. DRIFTS spectra of adsorbed pyridine at 373 K over (A) Pd/m-ZrO₂; (B) Pd/m,t-ZrO₂; (C) Pd/t-ZrO₂.

similar to that of the Pd/t-ZrO₂ catalyst. The remarkable difference is the lower intensity of the bands on the Pd/m-ZrO₂ and Pd/m,t-ZrO₂ catalysts, indicating a lower density of acid sites. Furthermore, the band at around 1592 cm⁻¹ is not observed in the presence of the monoclinic phase. It is important to stress that bands characteristic of Brønsted acid sites were not detected in the spectra of any catalyst.

The titration of oxophilic sites of Pd/ZrO₂ catalysts was determined by two different methods: temperature-programmed desorption of NH₃ (NH₃-TPD) and the cyclohexanol dehydration reaction. The NH₃-TPD profiles of the three catalysts are displayed in the Supporting Information (Figure S1). There was only one peak in the NH₃ desorption profile of Pd/ZrO₂ catalysts. For Pd/m-ZrO₂ and Pd/m,t-ZrO₂ the peak was observed at lower temperature (493 K) than in the TPD profile of Pd/t-ZrO₂ (558 K). These peaks correspond to weak acid sites. The density of oxophilic sites on Pd/m-ZrO₂, Pd/m,t-ZrO₂, and Pd/t-ZrO₂ catalysts was 0.94, 1.36, and 2.15 μmol·m⁻², respectively (Table 2).

The conversion of the cyclohexanol reaction was also used to characterize the acid–base properties of the zirconia support as it was previously proposed in the literature.²⁸ Duprez et al.²⁸ proposed to characterize the acid–base properties of oxides using the conversion of the cyclohexanol reaction. They reported that the dehydration of cyclohexanol to cyclohexene would likely be catalyzed by the acid sites, whereas the dehydrogenation of cyclohexanol to cyclohexanone is promoted by both acid and basic sites (formed by surface oxygen ions of the oxide lattice) through a concerted mechanism. In our work, the rate of cyclohexanol dehydration followed the order: Pd/m-ZrO₂ (10.9 mmol·min⁻¹·g_{cat}⁻¹), Pd/m,t-ZrO₂

Table 2. Total Amount of Ammonia Desorbed and Rate of Dehydration of the Cyclohexanol Reaction at 543 K for Fresh and Used Catalysts^b

catalyst	ammonia desorbed (μmol/m ²)	rate of OL dehydration (mmol/(min·g _{cat}))	
		fresh catalysts	used catalysts
Pd/m-ZrO ₂	0.94	10.9 (13.5) ^a	1.07
Pd/m,t-ZrO ₂	1.36	12.6 (10.8)	0.84
Pd/t-ZrO ₂	2.14	64.9 (13.9)	35.8

^aThe value in parentheses corresponds to the rate of cyclohexanol dehydrogenation at 543 K to cyclohexanone. ^bAfter HDO of the phenol reaction during 20 h TOS.

(12.6 mmol·min⁻¹·g_{cat}⁻¹) < Pd/t-ZrO₂ (64.9 mmol·min⁻¹·g_{cat}⁻¹) (Table 2). This result is in agreement with the NH₃-TPD experiment. Both techniques revealed that the Pd supported over t-ZrO₂ exhibited the highest density of oxophilic sites. The rate of cyclohexanol dehydrogenation was similar between the two catalysts (Table 2). Defect sites in proximity with metal particles have been suggested to catalyze dehydrogenation pathways in a number of reactions (e.g., metal/ceria catalysts for water–gas shift, steam-assisted formic acid decomposition, and steam reforming of ethanol).^{36–40} In fact, the XANES spectra revealed that the degree of reduction of the two polymorph catalysts was similar, which agrees with their similar rate of dehydrogenation.

The relationship between the zirconia structure and acidity is controversial in the literature. Many authors have found a higher amount of acid sites for monoclinic ZrO₂ compared to the tetragonal ZrO₂.^{19,41,42} However, the opposite was observed for Te et al. evaluating Saint-Gobain Norpro zirconia carriers.⁴³ In this case, the values of adsorbed NH₃ were 1.2 μmol·m⁻² (m-ZrO₂) and 2.2 μmol·m⁻² (t-ZrO₂), which were quite similar to the ones obtained in our work. Nonetheless, no significant difference on acidity was observed for ZrO₂ with different fractions of monoclinic and tetragonal phase.³¹ In spite of the general trend that m-ZrO₂ has a higher density of acid sites than t-ZrO₂, this may vary for the zirconia supported catalyst. For example, Foraita et al.²⁷ reported that the m-ZrO₂ exhibited a higher acid site concentration (2.5 μmol·m⁻²) than tetragonal zirconia (1.9 μmol·m⁻²). However, the addition of Ni to zirconia support decreased the acid site concentration of all Ni/ZrO₂ catalysts (Ni/m-ZrO₂: 1.6 μmol·m⁻²; Ni/t-ZrO₂: 1.5 μmol·m⁻²). They proposed that deposited Ni particles interact with and block Lewis acid sites. Higher acidity was also observed for Pt/t-ZrO₂.²⁶ In this case, the density of acid sites on Pt/t-ZrO₂ was about 1.5-fold higher than Pt/m-ZrO₂. The apparent contradictory results could be attributed to the pretreatment conditions.

In fact, different sites are present on the surface of zirconia such as hydroxyls, oxygen vacancies, coordinatively unsaturated Zr–O pairs, and Lewis acid sites (Zr³⁺, Zr⁴⁺).⁴⁴ For example, the IR spectroscopy of adsorbed CO at low temperature has been used to measure acidity of oxides. Bands in the range between 2200–2100 cm⁻¹ are attributed to CO adsorbed on Zr cations. However, the adsorption of CO over the zirconia cations can be inhibited by the hydroxyl groups,^{44–47} and this can in turn affect the titration of these sites depending on the treatment conditions of the sample. In addition, water is a product of the HDO reaction, and, thus, the surface of the support will be hydroxylated during the reaction. Therefore, the

IR of CO and methanol was used to provide further information about the surface of monoclinic and tetragonal zirconia.

The IR bands after reduction of Pd/ZrO₂ catalysts at 573 K are shown in Figure 6. The bands between 3800–3600 cm⁻¹

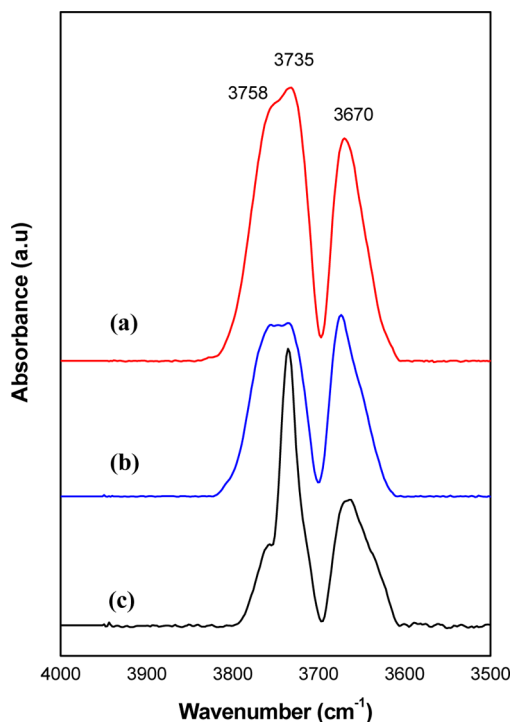


Figure 6. DRIFTS spectra of reduced catalysts at 573 K over (A) Pd/m-ZrO₂; (B) Pd/m,t-ZrO₂; (C) Pd/t-ZrO₂.

correspond to the O–H stretching vibrations of different types of surface hydroxyl groups. The band at 3758 cm⁻¹ is attributed to terminal OH groups, whereas the bands at 3735 and 3670 cm⁻¹ are assigned to bibriged and tribridged OH groups, respectively.^{44,48} The terminal and multicoordinated hydroxyl groups are observed for all zirconia samples, but their concentration is strongly dependent on zirconia structure. Comparing the spectra of Pd/m-ZrO₂ and Pd/t-ZrO₂, it is clear that the intensities of the bands at 3758 and 3670 cm⁻¹ for tetragonal zirconia are significantly lower than those of monoclinic zirconia. This result indicates that the surface of tetragonal zirconia is more dehydrated than that of the monoclinic one. The intensity of the bands of the Pd/m,t-ZrO₂ catalyst may not be directly compared due to its lower BET surface area.

The IR spectra after CO adsorption at 473 K are displayed in Figure 7a. According to the literature,⁴⁴ the weak IR band at 2183 cm⁻¹ is attributed to CO adsorbed on Zr⁴⁺, and the band at 2121 cm⁻¹ is due to CO adsorbed on Zr³⁺ cations. The bands at 2062 and 1960 cm⁻¹ are assigned to linear and bridge CO adsorption on metallic Pd particles.^{49–51} The bands between 1700–1200 cm⁻¹ are attributed to the different vibrational modes of monodentate and bidentate formate species:⁴⁴ 1570 and 1361 cm⁻¹ ($\nu(\text{OCO})$ symmetric and asymmetric); 1381 cm⁻¹ ($\delta(\text{CH})$). The shoulder at 1531 cm⁻¹ and the bands at 1623, 1420, and 1336 cm⁻¹ could be due to the formation of hydrogen carbonates and carbonates species.⁵² Formates are formed by the reaction between CO and defect-associated hydroxyl groups. The intensities of the bands corresponding to formates and carbonate species were lower for tetragonal zirconia, suggesting a lower population of these species. This result agrees with the lower hydroxylation degree of the Pd/t-ZrO₂ catalyst. In addition, the IR spectra in the O–

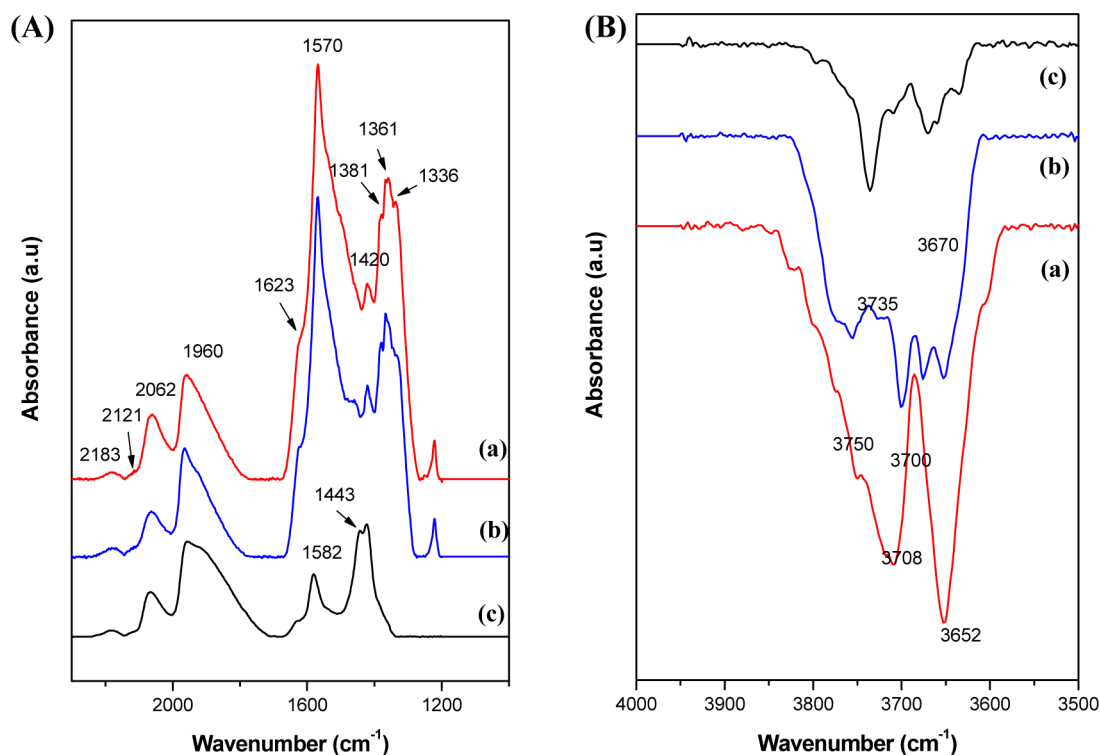


Figure 7. DRIFTS spectra of adsorbed CO at 473 K over (a) Pd/m-ZrO₂; (b) Pd/m,t-ZrO₂; (c) Pd/t-ZrO₂. (A) O–C stretching region; (B) O–H stretching region.

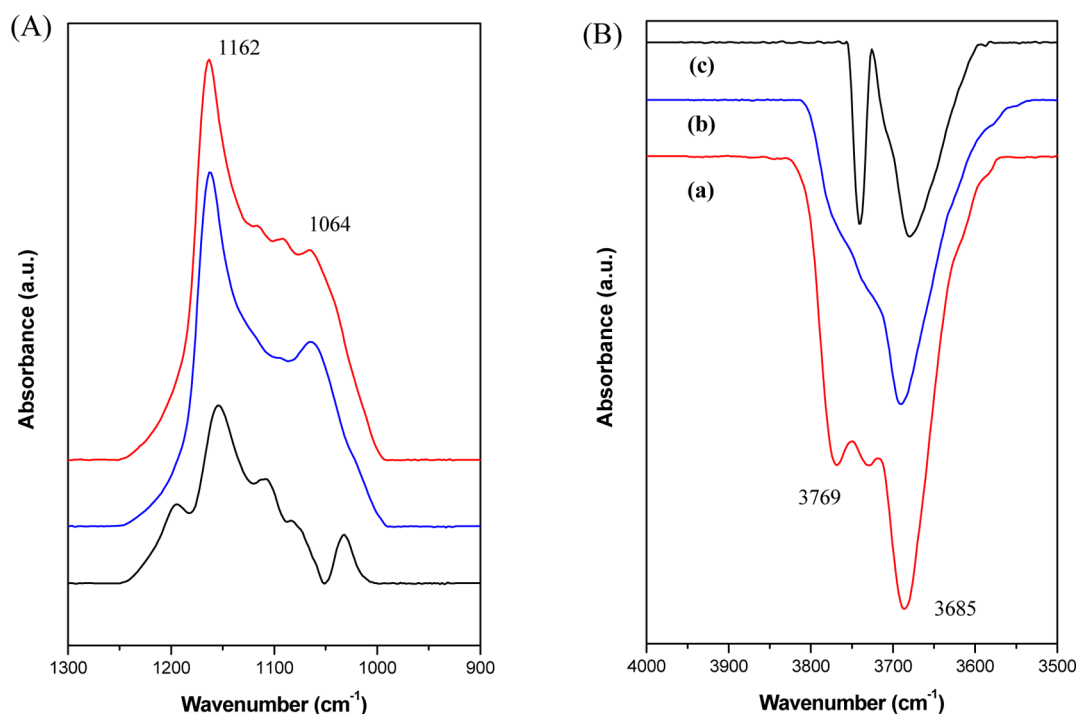


Figure 8. DRIFTS spectra of adsorbed methanol at 313 K over (a) Pd/m-ZrO₂; (b) Pd/m,t-ZrO₂; (c) Pd/t-ZrO₂. (A) O–C stretching region; (B) O–H stretching region.

H stretching region (Figure 7b) showed the presence of negative bands, which indicates that the hydroxyl groups reacted with CO producing formate species. The intensity of these bands followed the order: Pd/m-ZrO₂ > Pd/m,t-ZrO₂ > Pd/t-ZrO₂. This result confirms that the hydroxylation degree was higher for monoclinic zirconia.

Figure 8 shows the spectra obtained after adsorption of methanol at 313 K over Pd/ZrO₂ catalysts. The bands correspond to the different vibrational modes of methoxy species adsorbed on zirconia: 2925 and 2811 cm⁻¹ ($\nu_{\text{as}}(\text{CH}_3)$ and $\nu_{\text{s}}(\text{CH}_3)$) and 1162 and 1064 cm⁻¹ ($\nu_{\text{as}}(\text{O}-\text{C})$ and $\nu_{\text{s}}(\text{O}-\text{C})$).^{53,54} Methanol adsorbs dissociatively over metal oxide cation as a methoxy species in either monodentate or bidentate mode. In addition, it is observed the presence of negative bands in the O–H stretching region (3850–3600 cm⁻¹). Bianchi et al.⁵⁵ and Korhonen et al.⁵³ also reported a decrease of the intensities of the bands related to hydroxyl groups after adsorption of methanol that was attributed to the reaction between methanol in the gas phase and the defect-associated hydroxyl groups of the support, producing methoxy species. This reaction was more significant for monoclinic zirconia, suggesting a higher concentration of hydroxyl groups on the Pd/m-ZrO₂ catalyst.

Therefore, the IR of the reduced catalyst and CO and methanol adsorption revealed the surface of tetragonal zirconia may be more dehydrated than that of the monoclinic zirconia catalyst. Hadjiivanov and Lavalley⁴⁷ provided a simple model showing how hydroxylation of zirconia samples may block Lewis acid sites. Using that model as a basis to describe the current work, if the monoclinic zirconia catalyst is more hydroxylated, then zirconia cations on the tetragonal catalyst may be expected to be more accessible to reactants and intermediates during the HDO reaction. This perspective would be further supported by the higher density of oxophilic

sites as determined by DRIFTS of adsorbed pyridine, NH₃-TPD, and cyclohexanol dehydration probe reaction tests.

However, it should also be pointed out that the OH groups on ZrO₂ catalysts obtained were presumably formed by H₂ dissociation at the metal sites and spillover to the ZrO₂ support. In this scenario, –O_s species are expected to convert to –O_sH species. With this change, Zr⁴⁺ cations associated with –O_s species would be expected to undergo reduction to Zr³⁺ in order to accommodate the chemical change on the surface associated with –O_sH group formation. These defect-associated OH groups reacted with CO to form formate species during CO adsorption.

3.2. HDO of Phenol over Pd/ZrO₂ Catalysts. The HDO of the phenol reaction was performed over the supports (m-ZrO₂, m,t-ZrO₂, and t-ZrO₂). However, they did not exhibit any activity even at high W/F (0.16 h). Therefore, the catalyst activity should be attributed to either the metallic function or a bifunctional metal–support interaction. The phenol conversion and product yield as a function of W/F at 573 K over Pd/m-ZrO₂, Pd/m,t-ZrO₂, and Pd/t-ZrO₂ catalysts are shown in Figure 9. Concerning products yield, benzene and cyclohexanone were the main products formed over all catalysts. The amount of benzene increased with W/F, whereas the formation of cyclohexanone decreased. Traces of cyclohexanol and bicyclic compounds, typically C₁₂ compounds such as biphenyl, 2-phenylphenol, cyclohexylbenzene, 2-cyclohexylcyclohexan-1-one, and 2-cyclohexylphenol, were also formed at high W/F over all catalysts. The differences in product yields are more evident at low W/F. In this region, benzene formation was favored over Pd/t-ZrO₂, while cyclohexanone was the major product over Pd/m-ZrO₂. On the other hand, Pd/m,t-ZrO₂ exhibited an intermediate behavior; the amount of benzene is higher than that over Pd/m-ZrO₂ but still lower than that observed over Pd/t-ZrO₂. These differences are more clearly observed in Figure 10, which shows the selectivity to benzene

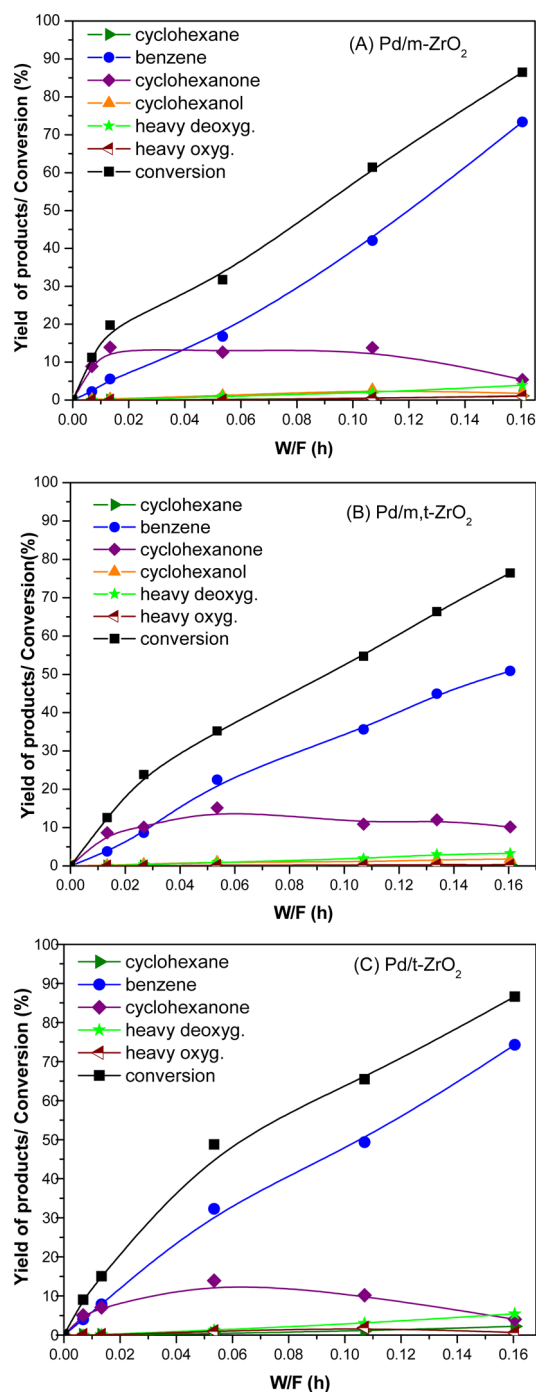


Figure 9. Phenol conversion and products yield as a function of W/F over (A) Pd/m-ZrO₂; (B) Pd/m,t-ZrO₂; and (C) Pd/t-ZrO₂.

and cyclohexanone as a function of phenol conversion. At low phenol conversion, the selectivity to cyclohexanone is higher than the selectivity to benzene for Pd/m-ZrO₂. The presence of a tetragonal phase in the Pd/m,t-ZrO₂ catalyst increased the formation of benzene. For the Pd/t-ZrO₂ catalyst, benzene was the main product for conversions of phenol higher than 20%. It is important to stress that the results obtained are far from the thermodynamic equilibrium under the reaction conditions used.

Table 3 compares the performance of these catalysts at low conversion level (around 10%). The reaction rate of Pd/t-ZrO₂ is 2-fold higher than that of Pd/m-ZrO₂. The selectivity to

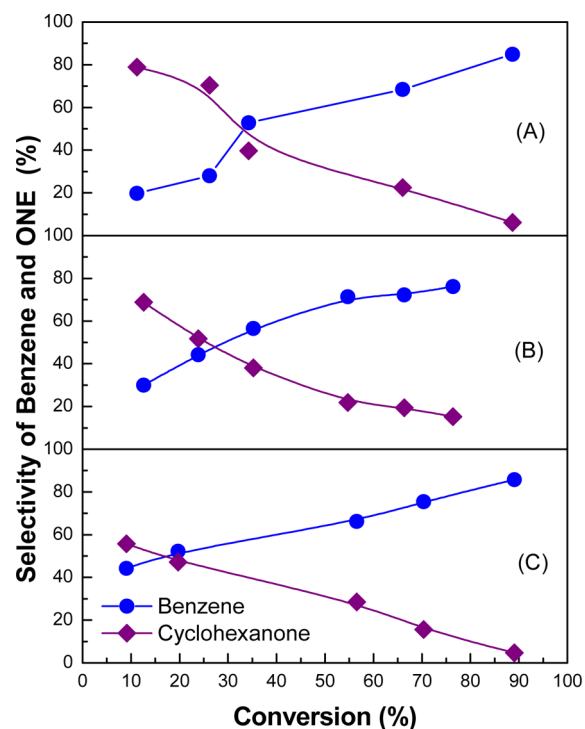


Figure 10. Selectivity to benzene and cyclohexanone as a function of phenol conversion over (A) Pd/m-ZrO₂; (B) Pd/m,t-ZrO₂; and (C) Pd/t-ZrO₂.

benzene increased in the order: Pd/m-ZrO₂ < Pd/m,t-ZrO₂ < Pd/t-ZrO₂. The selectivity to cyclohexanone followed the reverse order. Therefore, the zirconia morphology significantly affects the deoxygenation activity, and the tetragonal phase enhances HDO activity and promotes the selective pathway to benzene.

3.3. Cyclohexanol and Cyclohexanone Conversion over Pd/ZrO₂ Catalysts. Table 4 compares product yields for each feed at the same conversion level over Pd/ZrO₂ catalysts. The conversion of cyclohexanone over all catalysts yielded predominantly phenol and bicyclic compounds as the main products formed. Only small amounts of cyclohexanol and benzene were detected. Most of the benzene observed is likely produced as a secondary product from the direct conversion of phenol since phenol is the major product. The formation of C₁₂ compounds during the conversion of cyclohexanone has been reported in the literature.^{56,57} Bicyclic compounds are probably formed from the alkylation of phenolic and aromatic compounds by cyclohexanol or cyclohexanone, which is catalyzed by acid sites such as Lewis acid sites present on the supports.

The remarkable difference between the zirconia polymorphs was observed when cyclohexanol was used as the feed. For Pd/m-ZrO₂ and Pd/m,t-ZrO₂, cyclohexanone was the major product along with lower yields of phenol, benzene, and trace amounts of cyclohexane and cyclohexene. On the other hand, for Pd/t-ZrO₂, in addition to cyclohexanone, higher yields of cyclohexane, cyclohexene, and benzene were also observed. These products could be formed by two different reaction pathways: (i) the dehydration of cyclohexanol to cyclohexene followed by subsequent hydrogenation and dehydrogenation steps producing cyclohexane and benzene; (ii) the direct formation of benzene from phenol with cyclohexene and cyclohexane being produced from subsequent dehydration

Table 3. Product Distribution and Reaction Rate (TOF) for HDO of Phenol at 573 K^a

catalyst	conversion (%)	selectivity (%)			rate of reaction (mol/(min·g _{Pd}))
		benzene	ONE	OL	
Pd/m-ZrO ₂	11.2	19.7	78.9	1.4	0.029
Pd/m,t-ZrO ₂	12.6	29.9	68.7	1.3	0.026
Pd/t-ZrO ₂	9.1	44.2	55.7	0.0	0.056

^aONE: cyclohexanone; OL: cyclohexanol.

Table 4. Comparison of Performance of Pd/m-ZrO₂, Pd/m,t-ZrO₂, and Pd/t-ZrO₂ Catalysts and Respective Supports for Different Feeds^a

	W/F (h)	feed	yield (%)						
			ANE+ENE	BZ	ONE	OL	phenol	C ₁₂	X (%)
Pd/m-ZrO ₂	0.013	phenol	0.0	5.5	13.9	0.3		0.3	19.7
	0.023	ONE	0.1	2.0		2.2	13.2	6.8	24.3
	0.012	OL	1.0	3.3	11.5		6.1	0.0	21.9
m-ZrO ₂	0.160		5.8						5.8
	0.026	phenol	0.0	8.7	10.1	0.4		0.4	19.6
Pd/m,t-ZrO ₂	0.023	ONE	0.0	1.2		2.2	9.7	9.0	22.1
	0.024	OL	0.4	4.0	9.3		5.6	0.0	19.3
m,t-ZrO ₂	0.160		3.8						3.8
	0.013	phenol	0.0	10.3	9.2	0.0		0.0	19.5
Pd/t-ZrO ₂	0.023	ONE	0.7	2.0		0.9	7.8	7.5	18.9
	0.012	OL	5.4	6.6	8.4		2.1	0.1	22.5
t-ZrO ₂	0.160		97.0						97.0

^aANE: cyclohexane; ENE: cyclohexene; BZ: benzene; ONE: cyclohexanone; OL: cyclohexanol; C₁₂ compounds.

steps. In order to investigate the dehydration activity of the supports, cyclohexanol conversion over the bare supports was carried out at the highest W/F used for HDO of phenol. For m-ZrO₂ and m,t-ZrO₂ supports, the conversion of cyclohexanol was very low, indicating that the contribution of dehydration catalyzed by the support is negligible. Therefore, benzene should be directly formed from phenol. However, the t-ZrO₂ support was highly active for dehydration of cyclohexanol, producing mainly cyclohexene. Therefore, the formation of benzene by this reaction pathway over t-ZrO₂ support cannot be ruled out.

3.4. Effect of Zirconia Morphology on the Reaction Pathway. The HDO of phenol has been studied in the literature, and different reaction mechanisms are proposed.^{14,58,59} The direct deoxygenation (DDO) with cleavage of the Csp²-O bond by hydrogenolysis is widely used to explain the products formed during HDO of phenol. However, this reaction pathway is unlikely to proceed due to the high dissociation energy of the C-O bond of the aromatic ring.⁶⁰ The sequential hydrogenation (HYD) of the aromatic ring on metal sites to cyclohexanol followed by dehydration on acid sites and dehydrogenation to benzene on metal sites has also been reported in the literature.^{61,62} This reaction pathway requires a support with sufficient acidity to catalyze the dehydration of cyclohexanol. A third mechanism for HDO of phenol is based on the tautomerization of phenol to 2,4-cyclohexadienone.¹⁶ In this case, the support plays a key role in determining product distribution. In the case of supports with enough acidity like Al₂O₃, benzene might be formed by hydrogenation of the ring of the keto-tautomer intermediate, producing 2-cyclohexen-1-one that is hydrogenated to cyclohexanone and then cyclohexanol, which is dehydrated. For the Pd/ZrO₂ catalyst, the dehydration activity of the support is relatively low. Thus, the hydrogenation of the carbonyl group

preferentially occurs, leading to the formation of 3,5-cyclohexadienol, which can, in turn, convert to benzene. This selective hydrogenation of the carbonyl group is promoted by the oxophilic sites of zirconia, represented by incompletely coordinated Zr⁴⁺ cations (Lewis acid sites) near the perimeter of the metal particles. A stronger interaction between the oxygen atom in the phenol molecule with the oxophilic site favors the selective hydrogenation of the C=O of the keto-tautomer intermediate, promoting the formation of benzene.

In the present work, the zirconia morphology affected the reaction pathway. For the catalysts supported on m-ZrO₂ and m,t-ZrO₂, the hydrogenation of the carbonyl group seems to be the preferential route, whereas the hydrogenation of the ring might also occur over Pd/t-ZrO₂, since the dehydration of cyclohexanol occurs to a significant extent on t-ZrO₂. These results are likely related to the different density of oxophilic sites provided by each zirconia structure. DRIFTS of adsorbed pyridine, NH₃-TPD, and the dehydration of the cyclohexanol reaction revealed that the Pd/t-ZrO₂ catalyst possesses a higher density of oxophilic sites than Pd/m-ZrO₂ and Pd/m,t-ZrO₂. This was able to promote the dehydration of cyclohexanol formed, producing cyclohexene followed by the formation of benzene. The densities of oxophilic sites of Pd/m-ZrO₂ and Pd/m,t-ZrO₂ were lower, inhibiting the occurrence of this reaction pathway. In fact, the IR of adsorbed CO and methanol revealed that the surface of tetragonal zirconia is more dehydrated than the monoclinic one, and, thus, the oxophilic sites are less blocked by hydroxyl groups. Therefore, the oxophilic sites are more accessible to the phenol molecule during the HDO reaction over the Pd/t-ZrO₂ catalyst, which explains its higher activity to deoxygenated products.

3.5. Stability of Pd Catalysts on HDO of Phenol. Figure 11 shows the conversion of the phenol and product distribution as a function of time on stream (TOS) for the catalysts. The

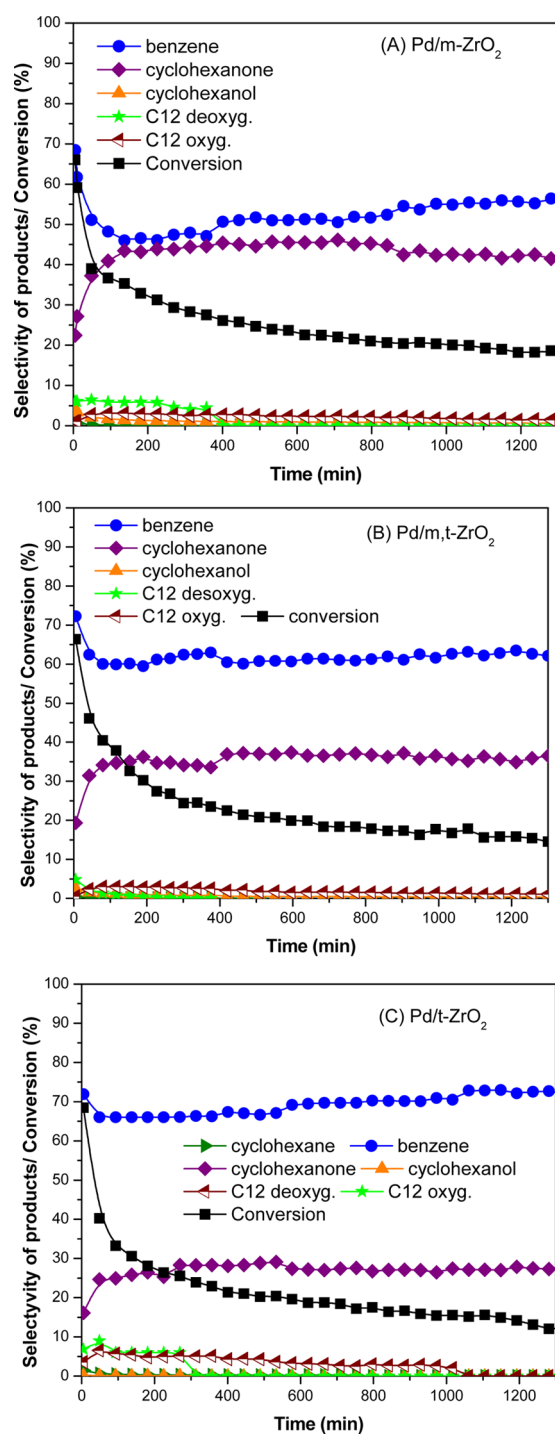


Figure 11. Conversion of phenol and selectivity to products as a function of TOS over (A) Pd/m-ZrO₂; (B) Pd/m,t-ZrO₂; and (C) Pd/t-ZrO₂.

initial phenol conversion was similar for all catalysts (around 65%) that significantly deactivated during 20 h of TOS. However, the deactivation degree was more significant for the Pd/t-ZrO₂ catalyst. Significant changes in the product distribution were observed with time. Benzene selectivity decreased, and the formation of cyclohexanone increased as the phenol conversion decreased for all catalysts. The selectivity to C₁₂ hydrocarbons decreased with TOS and they were no longer observed over Pd/m-ZrO₂ and Pd/m,t-ZrO₂, whereas it remained constant for the Pd/t-ZrO₂ catalyst.

The evolution of the adsorbed species formed during HDO of the phenol reaction was monitored by DRIFTS under reaction conditions.

The DRIFTS spectrum after 30 min under HDO of the phenol reaction over the Pd/m-ZrO₂ catalyst showed bands at 1283, 1430 (shoulder), 1487, 1587, 2858, 2934, 3026, and 3066 cm⁻¹ (Figure 12). These bands correspond to the different

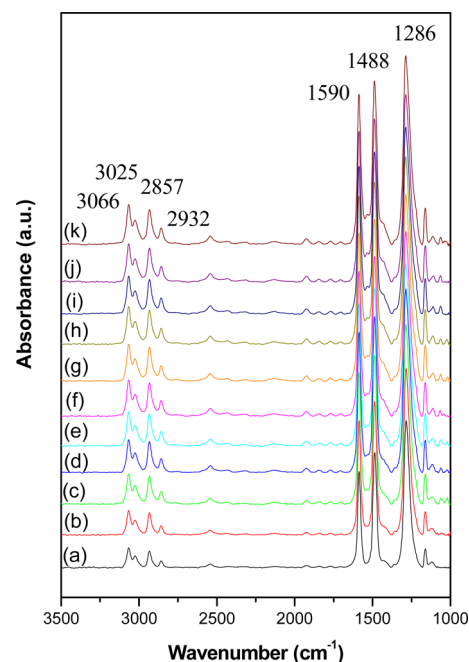


Figure 12. DRIFTS spectra obtained over the Pd/m-ZrO₂ catalyst at 573 K and under the reaction mixture containing the phenol + H₂ mixture during 6 h TOS: (a) 34; (b) 60; (c) 87; (d) 112; (e) 151; (f) 198; (g) 231; (h) 268; (i) 309; (j) 349; (k) 358 min.

vibrational modes of phenoxy and cyclohexanol species.¹⁶ It is noticed that the intensity of these bands increased continuously during 6 h TOS. Because these species are intermediates, the steadily increasing concentrations suggest that the reaction pathway for their selective turnover, which involves the metal–support junction, becomes impeded, resulting in an increasing inventory of intermediates on the oxide, where they form. That is, the increasing concentration of intermediates may be symptomatic of, but not the direct cause of, the deactivation.

The Pd/m,t-ZrO₂ catalyst exhibits a DRIFTS spectrum after 30 min of TOS very similar to the one obtained for the Pd/m-ZrO₂ catalyst, with bands at 1283, 1441, 1483, 1586, 2852, 2930, 3021, and 3064 cm⁻¹ (Figure S2). As it was previously discussed, these bands correspond to the different vibrational modes of phenoxy and cyclohexanol species. However, the intensities of these bands were weaker than those observed for monoclinic zirconia support. In this case, a strong increase in the band intensities was observed, which could also be attributed to a buildup of these species on the surface during 6 h of TOS.

For the Pd/t-ZrO₂ catalyst, it is noticed bands at 1274, 1422, 1486, 1587, 2857, 2933, and 3068 cm⁻¹ after 30 min of TOS (Figure 13). These bands also suggest the presence of phenoxy and cyclohexanol species on the surface. When the reaction time increased, not only did the intensities of these bands increase but also a new band appeared at 1656 cm⁻¹. This band has been assigned to the $\nu(\text{C}=\text{O})$ stretching mode of the

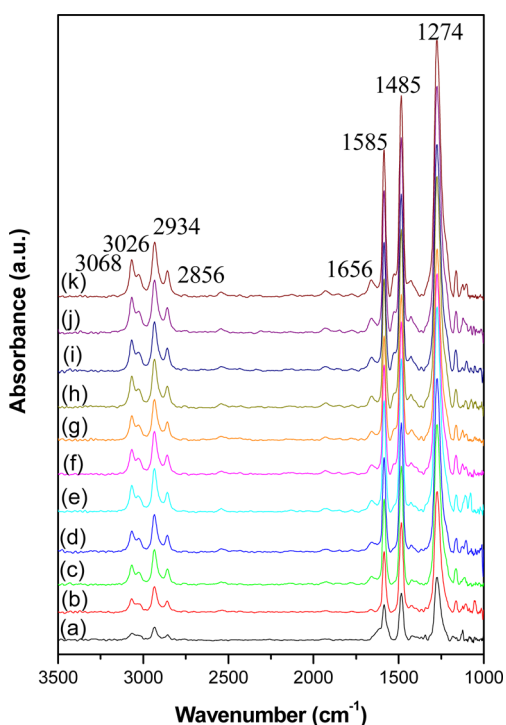


Figure 13. DRIFTS spectra obtained over the Pd/t-ZrO₂ catalyst at 573 K and under the reaction mixture containing the phenol + H₂ mixture during 6 h TOS: (a) 34; (b) 60; (c) 87; (d) 112; (e) 151; (f) 198; (g) 231; (h) 268; (i) 309; (j) 349; (k) 358 min.

adsorbed 2,4-cyclohexadien-1-one tautomer of phenol.¹⁶ This band was not observed on the Pd/m-ZrO₂ and Pd/m,t-ZrO₂ catalysts. The intensity of this band also increased during TOS. As it was suggested for the other zirconia supported catalysts, this result reveals an accumulation of reaction intermediates on the surface of the catalyst.

Therefore, the DRIFTS experiments under HDO of phenol for 6 h TOS showed the buildup of reaction intermediate species on the surface of Pd/ZrO₂ catalysts, regardless of the zirconia morphology. These results are in agreement with the long-term catalytic tests that showed a decrease in phenol conversion as well as benzene selectivity, the desired pathway that relies on the metal–support junction, while increases in the formation of 2,4-cyclohexadien-1-one and cyclohexanol were observed.

The reaction mechanism of HDO of phenol requires a metallic site for hydrogenation/dehydrogenation and an acid site that adsorbs the oxy compound and promotes dehydration, alkylation, and polymerization reactions. Recently, we demonstrated that the activity for deoxygenation depends on intimate contact between the metal and the oxophilic sites (Lewis acid sites). Therefore, the deactivation observed during the HDO of the phenol reaction is likely associated with the loss of the Pd-support interaction, which could be due to (i) carbon deposition resulting in site blocking at the interface; (ii) metal sintering, which decreases the interface between metal particles and support; or (iii) changes in the density of oxophilic sites of the support (e.g., decreases in Lewis acid sites due to site blocking by strong adsorbates).

In order to determine the main causes of catalyst deactivation, the used catalysts were characterized by Raman spectroscopy, thermogravimetric analysis (TG), cyclohexane dehydrogenation, and cyclohexanol dehydration. The Raman

spectra of the used catalysts did not detect the bands characteristic of carbon materials in the range of 1200–1800 cm⁻¹. In addition, carbon deposits on used catalysts were also not observed by TG analysis. Then, the deactivation of Pd/ZrO₂ catalysts was not caused by the coverage of Pd particles by carbonaceous deposits. In addition, comparing the Raman spectra of fresh and used catalysts did not reveal any changes in the structure of zirconia during the reaction.

To follow the changes in Pd dispersion, the dehydrogenation of the cyclohexane reaction was carried out after the reaction without exposure of the catalyst to air. Table 1 lists the Pd dispersion of the fresh and used catalysts after 20 h TOS. It is clear that the Pd dispersion significantly decreased during the reaction, indicating that the sintering of Pd particles is in large part responsible for catalyst deactivation. For the Pd/m-ZrO₂ catalyst, the changes in phenol conversion and dispersion were quite similar, indicating that sintering is likely the main cause of deactivation. However, the loss of activity during 20 h TOS was higher than the decrease in Pd dispersion for Pd/m,t-ZrO₂ and Pd/t-ZrO₂ catalysts, suggesting that changes in oxophilic site density could also be occurring. This result is in agreement with the changes observed in product distribution. The selectivity to benzene and bicyclic compounds decreased, whereas the selectivity to cyclohexanone increased as the catalyst deactivated. As previously discussed, the formation of bicyclic compounds takes place through alkylation of phenolic and aromatic compounds by cyclohexanol or cyclohexanone, which is catalyzed by acid sites such as Lewis acid sites present on the supports. Therefore, the loss of activity of Lewis acid sites for the alkylation reaction should lead to an increase in the selectivity of cyclohexanone and a decrease in the formation of C₁₂ hydrocarbons. In fact, the dehydration of cyclohexanol tests revealed that the density of oxophilic sites significantly decreased during the reaction (Table 2). The rate of the cyclohexanol dehydration reaction decreased 10–15-fold for Pd/m-ZrO₂ and Pd/m,t-ZrO₂ catalysts, whereas this reduction was less important for Pd/t-ZrO₂ (2-fold). This result agrees very well with the DRIFTS spectra under steady-state conditions that revealed an accumulation of phenoxy species during the reaction. The phenoxy species remained adsorbed on the Lewis acid sites, blocking those sites from further reactant adsorption.

Therefore, the deactivation of Pd/ZrO₂ catalysts during HDO of phenol could be attributed to decreases in the metal particle-support interface (Pd sintering) that lead to an increasing inventory of intermediate species on the surface of zirconia.

4. CONCLUSIONS

The zirconia morphology significantly affects the deoxygenation activity and selectivity to deoxygenated products during HDO of the phenol reaction. The Pd/t-ZrO₂ catalyst exhibited the highest activity for HDO and selectivity to benzene. Pd/m-ZrO₂ and Pd/t-ZrO₂ catalysts showed the same Pd dispersion but different density of acid sites. NH₃-TPD, dehydration of cyclohexanol, and DRIFTS of adsorbed pyridine revealed that the Pd supported on t-ZrO₂ has the highest density of oxophilic sites. In fact, the IR of the reduced catalyst and CO and methanol adsorption revealed that zirconia cations appear to be more accessible to phenol molecules during the HDO reaction for Pd/t-ZrO₂ relative to Pd/m-ZrO₂. This difference in the density of oxophilic sites affected the reaction pathway over zirconia supported Pd catalysts. For Pd/t-ZrO₂, the support has

enough acidity to promote the dehydration of cyclohexanol formed to cyclohexene, followed by the formation of benzene. Thus, benzene might be formed by hydrogenation of the aromatic ring as well as by hydrogenation of the carbonyl group over Pd/t-ZrO₂. In the case of Pd/m-ZrO₂ and Pd/m,t-ZrO₂ catalysts, the dehydration activity of the support is low, and this reaction pathway does not occur. Therefore, the formation of benzene likely takes place by an alternative route that involves the tautomerization of phenol to a cyclohexadienone intermediate.

Pd/ZrO₂ catalysts significantly deactivated with time. The dehydrogenation of cyclohexane and dehydration of cyclohexanol showed that the Pd particle size increased and the density of acid sites decreased during the HDO of the phenol reaction. In addition, the DRIFTS spectra under reaction conditions demonstrated that phenoxy and intermediate species accumulated during the reaction. Losses in the Pd-support interface responsible for the selective pathway to benzene occurred, resulting in a steadily increasing inventory of intermediates on the oxide surface with time on stream. This in turn resulted in a covering of oxophilic sites by the intermediates as a result of the narrowing bottleneck of the selective route. These species thus remained adsorbed on the oxophilic sites, blocking those sites and inhibiting further reactant adsorption. Therefore, the steady growth of Pd particles is likely responsible for the losses in the metal-support interface with TOS, leading to catalyst deactivation and a decrease in the density of available oxophilic sites.

■ ASSOCIATED CONTENT

● Supporting Information

The Supporting Information is available free of charge on the ACS Publications website at DOI: 10.1021/acscatal.5b01501.

NH₃-TPD profiles of Pd/m-ZrO₂, Pd/m,t-ZrO₂, and Pd/t-ZrO₂ and DRIFTS spectra obtained over the Pd/m,t-ZrO₂ catalyst at 573 K and under the reaction mixture containing the phenol + H₂ mixture during 6 h TOS (PDF)

■ AUTHOR INFORMATION

Corresponding Author

*E-mail: fabio.bellot@int.gov.br.

Notes

The authors declare no competing financial interest.

■ ACKNOWLEDGMENTS

Support from the National Science Foundation (EP-SCoR0814361), US Department of Energy (DE-FG36G088064), Oklahoma Secretary of Energy, and the Oklahoma Bioenergy Center are greatly appreciated. Priscilla M. de Souza thanks CAPES (Coordenação de Aperfeiçoamento de Pessoal de Ensino Superior) for financial support. The group thanks the LNLS (Brazilian Synchrotron Light Laboratory) for the assigned beamtime at XAFS-1 and for the valuable support to perform the XAFS studies. The authors thank Saint-Gobain NorPro for providing the zirconia materials. CAER researchers acknowledge support from the Commonwealth of Kentucky.

■ REFERENCES

- (1) Han, Y.; Zhu, J. *Top. Catal.* **2013**, *56*, 1525–1541.
- (2) Hsu, Y.-S.; Wang, Y.-L.; Ko, A.-N. *J. Chin. Chem. Soc.* **2009**, *56*, 314–322.
- (3) Duan, H.; Sun, D.; Yamada, Y.; Sato, S. *Catal. Commun.* **2014**, *48*, 1–4.
- (4) Zhang, Q.; Yin, Z.; Haitao, L.; Yongxiang, Z.; Meng, M.; Yu, Y. *Chin. J. Catal.* **2013**, *34*, 1159–1166.
- (5) Panchenko, V. N.; Zaytseva, Y. A.; Simonov, M. N.; Simakova, I. L.; Paukshtis, E. A. *J. Mol. Catal. A: Chem.* **2014**, *388–389*, 133–140.
- (6) Zaytseva, Y. A.; Panchenko, V. N.; Simonov, M. N.; Shutilov, A. A.; Zenkovets, G. A.; Renz, M.; Simakova, I. L.; Parmon, V. N. *Top. Catal.* **2013**, *56*, 846–855.
- (7) Chen, C.; Ruan, C.; Zhan, Y.; Lin, X.; Zheng, Q.; Wei, K. *Int. J. Hydrogen Energy* **2014**, *39*, 317–324.
- (8) Hakeem, A. A.; Li, M.; Berger, R. J.; Kapteijn, F.; Makkee, M. *Chem. Eng. J.* **2015**, *263*, 427–434.
- (9) Sintarako, P.; Praserttham, P.; Thammongkol, V.; Pokacharoenwatjana, B.; Yuanglamyai, W.; Inthiwong, C. *Catal. Commun.* **2015**, *62*, 89–94.
- (10) Zhang, X.; Wang, T.; Ma, L.; Zhang, Q.; Huang, X.; Yu, Y. *Appl. Energy* **2013**, *112*, 533–538.
- (11) Ohta, H.; Feng, B.; Kobayashi, H.; Hara, K.; Fukuoka, A. *Catal. Today* **2014**, *234*, 139–144.
- (12) Yakovlev, V. A.; Khromova, S. A.; Sherstyuk, O. V.; Dundich, V. O.; Ermakov, D. Y.; Novopashina, V. M.; Lebedev, M. Y.; Bulavchenko, O.; Parmon, V. N. *Catal. Today* **2009**, *144*, 362–366.
- (13) Bui, V. N.; Laurenti, D.; Delichère, P.; Geantet, C. *Appl. Catal., B* **2011**, *101*, 246–255.
- (14) Mortensen, P. M.; Grunwaldt, J.-D.; Jensen, P. A.; Jensen, A. D. *ACS Catal.* **2013**, *3*, 1774–1785.
- (15) de Souza, P. M.; Nie, L.; Borges, L. E. P.; Noronha, F. B.; Resasco, D. E. *Catal. Lett.* **2014**, *144*, 2005–2011.
- (16) de Souza, P. M.; Rabelo-Neto, R. C.; Borges, L. E. P.; Jacobs, G.; Davis, B. H.; Sooknoi, T.; Resasco, D. E.; Noronha, F. B. *ACS Catal.* **2015**, *5*, 1318–1329.
- (17) Bokhimi, X.; Munoz, E.; Boldú, J. L.; Adem, E.; Novaro, O. J. *Sol-Gel Sci. Technol.* **2000**, *17*, 219–225.
- (18) Purwasmita, B. S.; Larasati, L. D.; Septawendar, R.; Nugraha, A. B.; Aufan, M. R.; Sosiati, H. *J. Aust. Ceram. Soc.* **2013**, *49*, 89–94.
- (19) Zhao, Y.; Li, W.; Zhang, M.; Tao, K. *Catal. Commun.* **2002**, *3*, 239–245.
- (20) Bachiller-Baeza, B.; Ramos, R.; Ruiz, A. G. *Langmuir* **1998**, *14*, 3556–3564.
- (21) Pokrovski, K.; Jung, K. T.; Bell, A. T. *Langmuir* **2001**, *17*, 4297–4303.
- (22) Ma, Z. Y.; Yang, C.; Wei, W.; Li, W. H.; Sun, Y. H. *J. Mol. Catal. A: Chem.* **2005**, *227*, 119–124.
- (23) Jung, K. T.; Bell, A. T. *Catal. Lett.* **2002**, *80*, 63–68.
- (24) Benito, M.; Padilla, R.; Rodríguez, L.; Sanz, J. L.; Daza, L. *J. Power Sources* **2007**, *169*, 167–176.
- (25) Campa, M. C.; Ferraris, G.; Gazzoli, D.; Pettiti, I.; Pietrogiamici, D. *Appl. Catal., B* **2013**, *142–143*, 423–431.
- (26) Hellinger, M.; Carvalho, H. W. P.; Baier, S.; Wang, D.; Kleist, W.; Grunwaldt, J. D. *Appl. Catal., A* **2015**, *490*, 181–192.
- (27) Foraita, S.; Fulton, J. L.; Chase, Z. A.; Vjunov, A.; Xu, P.; Baráth, E.; Camaioni, D. M.; Zhao, C.; Lercher, J. A. *Chem. - Eur. J.* **2015**, *21*, 2423–2434.
- (28) Martin, D.; Duprez, D. *J. Mol. Catal. A: Chem.* **1997**, *118*, 113–128.
- (29) Boudart, M. *Adv. Catal.* **1969**, *20*, 153–166.
- (30) Passos, F. B.; Oliveira, E. R.; Mattos, L. V.; Noronha, F. B. *Catal. Today* **2005**, *101*, 23–30.
- (31) Khaodee, W.; Jongsomjit, B.; Prasertthama, P.; Goto, S.; Assabumrungrat, S. *J. Mol. Catal. A: Chem.* **2008**, *280*, 35–42.
- (32) Li, P.; Chen, I.-W.; Penner-Hahn, J. E. *Phys. Rev. B: Condens. Matter Mater. Phys.* **1993**, *48*, 10063–10073.
- (33) Meneghetti, F.; Wendel, E.; Mascotto, S.; Smarsly, B. M.; Tondello, E. *CrystEngComm* **2010**, *12*, 1639–1649.
- (34) Penkova, A.; Bobadilla, L. F.; Romero-Sarria, F.; Centeno, M. A.; Odriozola, J. A. *Appl. Surf. Sci.* **2014**, *317*, 241–251.
- (35) Binet, C.; Daturi, M.; Lavalley, J. C. *Catal. Today* **1999**, *50*, 207–225.

- (36) Jacobs, G.; Graham, U. M.; Chenu, E.; Patterson, P. M.; Dozier, A.; Davis, B. H. *J. Catal.* **2005**, *229*, 499–512.
- (37) Jacobs, G.; Ricote, S.; Graham, U. M.; Patterson, P. M.; Davis, B. H. *Catal. Today* **2005**, *106*, 259–264.
- (38) Jacobs, G.; Patterson, P. M.; Graham, U. M.; Crawford, A. C.; Davis, B. H. *Int. J. Hydrogen Energy* **2005**, *30*, 1265–1276.
- (39) Jacobs, G.; Patterson, P. M.; Graham, U. M.; Crawford, A. C.; Dozier, A.; Davis, B. H. *J. Catal.* **2005**, *235*, 79–91.
- (40) Jacobs, G.; Keogh, R. A.; Davis, B. H. *J. Catal.* **2007**, *245*, 326–337.
- (41) Jung, K. T.; Shul, Y. G.; Bell, A. T. *Korean J. Chem. Eng.* **2001**, *18* (6), 992–999.
- (42) Gijjupalli, S. R.; Mugawar, S.; Rajan, P.; Balla, P. K.; Komandur, V. R. C. *Appl. Surf. Sci.* **2014**, *309*, 153–159.
- (43) Te, M.; Dahar, S.; Koradia, P.; Ono, Y. *Sci. Technol. Catal.* **2006**, *172*, 133–136.
- (44) Kouva, S.; Honkala, K.; Lefferts, L.; Kanervo. *Catal. Sci. Technol.* **2015**, *5*, 3473–3490.
- (45) Bianchi, D.; Chafik, T.; Khalfallah, M.; Teichner, S. *J. Appl. Catal., A* **1993**, *105*, 223–249.
- (46) Kouva, S.; Andersin, J.; Honkala, K.; Lehtonen, J.; Lefferts, L.; Kanervo, J. *Phys. Chem. Chem. Phys.* **2014**, *16*, 20650–20664.
- (47) Hadjiivanov, K.; Lavalley, J.-C. *Catal. Commun.* **2001**, *2*, 129–133.
- (48) Rhodes, M. D.; Bell, A. T. *J. Catal.* **2005**, *233*, 198–209.
- (49) Mojet, B. L.; Miller, J. T.; Koningsberger, D. C. *J. Phys. Chem. B* **1999**, *103*, 2724–2734.
- (50) Hicks, R. F.; Yen, Q.; Bell, A. T. *J. Catal.* **1984**, *89*, 498–510.
- (51) Vannice, M. A.; Wang, S.-Y. *J. Phys. Chem.* **1981**, *85*, 2543–2546.
- (52) Binet, C.; Daturi, M.; Lavalley, J. C. *Catal. Today* **1999**, *50*, 207–225.
- (53) Korhonen, S. T.; Banares, M. A.; Fierro, J. L. G.; Krause, A.O. I. *Catal. Today* **2007**, *126*, 235–247.
- (54) Jung, K. T.; Bell, A. T. *Top. Catal.* **2002**, *20*, 97–105.
- (55) Bianchi, D.; Chafik, T.; Khalfallah, M.; Teichner, S. *J. Appl. Catal., A* **1995**, *123*, 89–110.
- (56) Nimmanwudipong, T.; Runnebaum, R. C.; Tay, K.; Block, D. E.; Gates, B. C. *Catal. Lett.* **2011**, *141*, 1072–1078.
- (57) Zhao, C.; Camaioni, D. M.; Lercher, J. A. *J. Catal.* **2012**, *288*, 92–103.
- (58) Echeandia, S.; Pawelec, B.; Barrio, V. L.; Arias, P. L.; Cambra, J. F.; Loricera, C. V.; Fierro, J. L. G. *Fuel* **2014**, *117*, 1061–1073.
- (59) Newman, C.; Zhou, X.; Goundie, B.; Ghampson, I. T.; Pollock, R. A.; Ross, Z.; Wheeler, M. C.; Meulenberg, R.; Austin, R. N.; Frederick, B. G. *Appl. Catal., A* **2014**, *477*, 64–74.
- (60) Furimsky, E. *Appl. Catal., A* **2000**, *199*, 147–190.
- (61) Echeandia, S.; Arias, P. L.; Barrio, V. L.; Pawelec, B.; Fierro, J. L. G. *Appl. Catal., B* **2010**, *101*, 1–12.
- (62) Zhao, C.; He, J.; Lemonidou, A. A.; Li, X.; Lercher, J. J. *J. Catal.* **2011**, *280*, 8–16.